Target deconvolution of HDAC pharmacopoeia highlights MBLAC2 as common off-target

Severin Lechner
Chair of Proteomics and Bioanalytics, TUM School of Life Sciences, Technical University of Munich
Martin Malgapo
Department of Molecular Medicine, College of Veterinary Medicine, Cornell University
Christian Grätz
Animal Physiology and Immunology, TUM School of Life Sciences, Technical University of Munich
https://orcid.org/0000-0002-9356-7940
Agnes Baron
Chair of Proteomics and Bioanalytics, TUM School of Life Sciences, Technical University of Munich
Patrick Leopold Rüther
Novo Nordisk Foundation Center for Protein Research https://orcid.org/0000-0003-4461-9828
Simon Nadal
Chair of Proteomics and Bioanalytics, TUM School of Life Sciences, Technical University of Munich
Carmen Stumpf
Chair of Proteomics and Bioanalytics, TUM School of Life Sciences, Technical University of Munich
Christina Loos
Chair of Proteomics and Bioanalytics, TUM School of Life Sciences, Technical University of Munich
Xin Ku
Shanghai Jiao Tong University
Polina Prokofeva
Chair of Proteomics and Bioanalytics, TUM School of Life Sciences, Technical University of Munich
Ludwig Lautenbacher
Computational Mass Spectrometry, TUM School of Life Sciences, Technical University of Munich
Tino Heimburg
Institute of Pharmacy, Martin Luther University of Halle-Wittenberg, Halle/Saale, Germany
Vivian Würf
6) LipiTUM, Chair of Experimental Bioinformatics, TUM School of Life Sciences, Technical University of Munich
Chen Meng
TUM
Wolfgang Sippl
https://orcid.org/0000-0002-5985-9261
Mathias Wilhelm

TU Munich https://orcid.org/0000-0002-9224-3258

Karin Kleigrewe

Bavarian Center for Biomolecular Mass Spectrometry (BayBioMS), Technical University of Munich

Josch Pauling

LipiTUM, Chair of Experimental Bioinformatics, TUM School of Life Sciences, Technical University of Munich

Karl Kramer

Chair of Proteomics and Bioanalytics, TUM School of Life Sciences, Technical University of Munich

Michael Pfaffl

Animal Physiology and Immunology, TUM School of Life Sciences, Technical University of Munich

Maurine Linder

Cornell University https://orcid.org/0000-0003-2202-9712

Bernhard Kuster

Chair of Proteomics and Bioanalytics, Technical University Munich https://orcid.org/0000-0002-9094-1677

Guillaume Médard (g.medard@tum.de)

Chair of Proteomics and Bioanalytics, TUM School of Life Sciences, Technical University of Munich https://orcid.org/0000-0002-4782-4029

Article

Keywords: HDAC drugs, drug discovery, chemical proteomics

Posted Date: July 12th, 2021

DOI: https://doi.org/10.21203/rs.3.rs-646613/v1

Abstract

HDAC drugs have entered the pharmacopoeia in the 2000s. However, some enigmatic phenotypes suggest off-target engagement. Here, we developed a chemical proteomics assay using three promiscuous chemotypes and quantitative mass spectrometry that we deployed to establish the target landscape of 53 drugs. The results highlight 14 direct targets, including 9 out of the 11 human zinc-dependent HDACs, question the reported selectivity of widely-used molecules, notably for HDAC6, and delineate how the composition of HDAC complexes influences drug potency. Unexpectedly, metallo-beta-lactamase domain-containing protein 2 (MBLAC2) featured as a frequent target of hydroxamate drugs. This ill-annotated palmitoyl-CoA hydrolase is inhibited by 24 HDAC inhibitors at low nM potency. Both enzymatic inhibition and knocking down the protein led to the accumulation of extracellular vesicles. Given the importance of exosome biology in neurological diseases or cancer, this HDAC-independent drug effect creates the incentive for considering MBLAC2 as a target for drug discovery.

Main Text

Inhibition of histone deacetylases (HDACs) has emerged as a promising therapeutic option in oncology as well as further conditions such as Duchenne Muscular Dystrophy[1]. The FDA-approval of the first-in-class HDAC inhibitor (HDACi) Vorinostat in 2006 for the treatment of cutaneous T-cell lymphoma[2] marked the start of a series of drug approvals for cancerous diseases. Notably, most clinical HDACis engage several HDACs from all human phylogenetic branches designating them as pan-HDACis. Such polypharmacological mechanisms of action (MoA) might be beneficial particularly in oncology, where multiple disease-relevant class I and II HDACs are inhibited simultaneously[3, 4]. However, conditions such as Amyotrophic Lateral Sclerosis or Huntington's Disease would require class II isoform-selective inhibitors that precisely interfere with the pathologic mechanism[5-8] but bypass the toxicity arising from inhibition of epigenetic class I HDACs[9-11]. Therefore, the delineation of the target spectrum of HDACis appears essential for the understanding of their MoAs and for the development of more bespoke therapies.

HDAC activity highly depends on their molecular context such as post-translational modifications (PTMs)[12, 13], allosteric factors[14, 15] or participation in gene regulatory protein complexes[16]. These factors have been shown to impact drug affinity but are not recapitulated in traditional enzyme activity assays[17, 18]. To address this challenge, a landmark study by Bantscheff et al.[17] reported a chemoproteomic assay that probes HDACi target engagement in lysates containing natively folded proteins, their cofactors and maintaining biomolecular interactions. The immobilization of Vorinostat allowed for the pulldown of HDAC complexes and competitive drug binding enabled the selectivity profiling of 16 HDACis against 6 of the 11, more particularly class I and IIb, HDACs. These chemoproteomics experiments led to the discovery of the Mitotic Deacetylase Complex (MiDAC), which was later shown to be relevant for correct mitotic chromosome alignment[19]. Moreover, the study revealed that aminoanilide-based HDACis exhibit reduced affinity for the Sin3 HDAC-complex and slow binding kinetics[17, 18]. So far, however, promiscuous affinity

matrices designed to profile HDAC drugs do not address class IIa HDACs[20], which are targets of rising interest[7, 8, 21, 22].

Here, we substantially extended the existing profiling technology by creating an affinity matrix able to enrich 9 of 11 Zn^{2+}-dependent HDACs (Zn-HDACs), now including class IIa, and mapped the target landscape of 53 HDAC and metallohydrolase drugs. The results highlight HDACis with unexpected target profiles and low selectivity. However, we also identify drugs with unparalleled selectivity for HDAC10 and HDAC6. Moreover, the quantitative data revealed that drugs interacting with the CoREST complex variants containing either RCOR1 or RCOR3 show larger than ten-fold difference in HDAC1 binding affinity. Surprisingly, about half of the HDACis, including clinically advanced molecules, inhibit metallo-beta-lactamase domain-containing protein 2 (MBLAC2)[23] at nano-molar concentrations. We further demonstrate that pharmacological inhibition or knockdown of MBLAC2 triggers accumulation of extracellular vesicles in cell culture, placing this poorly characterized protein into the context of extracellular vesicle biology.

Results

New chemical affinity probes allow for chemoproteomic profiling against 9 of 11 Zn-HDACs. Inspired by the pharmacophores of HDAC drugs, we synthesized 15 chemical probes (**1 – 15)** (Fig. 1a) and evaluated their suitability for enriching HDACs from lysates of ten cell lines (Fig. S1 and S2). Combining probes iC, iQ and iA for pulldowns from mixed lysates of MV4-11 and SW620 cells showed the best overall results: iC robustly enriched seven HDACs including class IIa HDAC4,5 and 7 as well as MBLAC2 (Fig. 1b, Fig. S1b,c). Addition of iQ improved the enrichment of HDAC3 and HDAC8 (Fig. 1b), extending the coverage of the affinity matrix to 9 of the 11 Zn-HDACs. We also included iA, since we observed that it enriched many metalloenzymes, including iron-sulfur cluster proteins (Fig. S2, Fig. 1b) as well as GATD3A, ALDH2, ISOC1, ISOC2 that later unravelled as common HDACi off-targets (see below).

With such an affinity matrix, the target profiles of drugs can be obtained by competition experiments. Here, the drug of interest is added in increasing doses to the lysate where it engages its targets and prevents specific binding of the same targets to the matrix in a dose-dependent fashion (Fig. S3). Plotting the relative intensities of matrix-binding proteins over increasing doses of free drug allows derivation of EC_{50} and apparent K_d values (K_d^{app}) that characterize the interaction (see methods). Importantly, binding equilibrium between the molecule and the targets is essential to obtain meaningful K_d^{app} values. To account for the slow on-rates of the aminoanilide-based inhibitors[18, 24], we evaluated incubation temperatures of 4 °C and 22 °C (i.e. room temperature) and times ranging from 0 to 1485 min for two exemplary HDACis set to compete at 30 µM. While hydroxamic acid CHDI00465983 engaged with class IIa HDACs within a few minutes both at 4 °C and 22 °C, 30-60 minutes incubation at room temperature was required for aminoanilide Entinostat to show full competition (Fig. 1c, Fig. S4), consistent with its reported extremely slow k_{on} rate[18]. We then validated a protocol with a 90 min total incubation (60 min drug pre-incubation and 30 min pulldown) at 30 °C that could accommodate for very slow binders. Here,

we profiled Trichostatin A, Mocetinostat, Vorinostat, Romidepsin, and Panobinostat and compared the results to previously published large scale HDACi profiling studies (Fig. S5)[17, 24, 25]. Dose responses of Romidepsin showed competition of HDACs from class I, IIb and IIa (Fig. 1d) and pK_d^{app} values correlated well with enzyme activity assay[25] (Fig. 1e) and BRET-based in-cell target engagement data[24] (Fig. S5). We found lower correlation with the initial chemoproteomics study by Bantscheff and co-authors[17]. In particular, slow binder Mocetinostat showed higher affinities here than originally published (Fig. S5)[17]. However, the authors have acknowledged their initial affinity underestimation of aminoanilides in a later study, where they optimized the incubation conditions[18]. Remarkably, our K_d^{app}s for Panobinostat correlated extremely well (R^2 = 0.92) to their more recent study using immobilised Panobinostat (Fig. S5)[26].

The target landscape of HDAC drugs. We next profiled 53 molecules comprising the majority of all clinical HDAC drugs, several HDAC tool compounds and five hydroxamate-based metallohydrolase drugs (see Fig. S6 for structures). Only a few vignettes of the data can be highlighted in this manuscript but the complete profiling data can be dynamically explored via ProteomicsDB (https://www.proteomicsdb.org/)[27-29]. Neither the HDAC activity modulator Tasquinimod nor the five metallohydrolase inhibitors (Batimastat, Ilomastat, Prinomastat, Marimastat, and Salicylhydroxamic acid) bound HDACs or other enriched metalloproteins with K_d^{app} values below 30 µM. Somewhat surprisingly, four HDACis (Resminostat, BRD73954, HPOB, and TH147) did not show any binding to HDACs or other proteins at concentrations of up to 30 µM either. Expectedly, Valproic and Phenylbutanoic acid displayed weak three-digit micromolar affinities (Table S1). Clustering of the remaining 41 drugs that have at least one micromolar target protein (40 designated HDAC inhibitors and Bufexamac) organized the compounds into four major groups (Fig. 2a, Table S1). Group A assembles the aminoanilides that are selective for binding HDAC1/2/3 only. Group B comprises the unique thiolate Romidepsin and hydroxamic acid-based pan-HDACis that often also engage MBLAC2. Group C features rather unselective HDACis (including approved and clinical drugs such as Vorinostat) that also bind non-HDAC off-targets, notably ALDH2 and the uncharacterized proteins ISOC1, ISOC2, and GATD3A. Group D, in contrast to groups A-C, is characterized by drugs that do not engage HDAC1/2/3. It includes the most selective and potent class IIa inhibitors CHDI00390576 and CHDI00465983 which primarily target HDAC5 and HDAC7 as well as TMP195, with preferred binding for HDAC7 over HDAC4 and HDAC5. Unsurprisingly, live-cell imaging of SW620 colorectal cancer cell drug treatment (at 100 nM and 1 µM) highlighted the most potent HDAC1/2/3 inhibitors of groups A-C to impact cell vitality, while group D drugs did not induce an altered cell morphology (Fig. S7). Exploring this landscape from a target perspective, 29 compounds (>50% of the total) bound class I HDACs, reflecting the efforts expended in developing therapeutic modulators of these targets and 26 molecules bound class IIb HDACs. In contrast, only 6 drugs targeted class IIa HDACs. Interestingly, MC1568 and LMK235, which are frequently used as class IIa-specific probes, showed no class IIa target engagement at all in our assay, questioning their use as chemical probes but rationalising the poor HDAC enrichment by probes based on these molecules (Fig. 2 and S1d).

Selectivity of HDAC inhibitors. The chemical proteomics data assembled here provided an opportunity to assess the selectivity of the HDACis for their targets. As a metric, we used the concentration- and target-dependent selectivity (CATDS) score[30], which compares the half maximal target engagement of a particular drug (i.e. a value of 0.5 for the pK_d^{app} of a drug:target interaction) to the level of target engagement of all targets at that same drug concentration (Fig. S8). Systematic CATDS calculation for all drugs and targets confirmed PCI-34051 as the only selective HDAC8 inhibitor[31] (Fig. 2b, Table S2). Surprisingly, our analysis revealed TH65 as a selective inhibitor for HDAC10 (CATDS = 0.83, pK_d^{app} = 6.2) (Fig. 2c). TH65 was designed as an inhibitor of *Schistosoma Mansoni* HDAC8 but not tested for human HDAC10 inhibition[32, 33]. Since no highly selective HDAC10 probes have been reported yet according to ChemicalProbes.org, our data designates TH65, with at least 30-fold selectivity (limit of our assay) over other HDACs, as novel promising chemical probe for HDAC10. Interestingly, we found the HDAC6 inhibitor Tubastatin A to be the second most selective HDAC10 inhibitor (CATDS = 0.67), contrasting the original and recent reports[34, 35] but agreeing with results of in-cell nano-BRET binding assays[36]. Furthermore, the pan-HDAC inhibitor Abexinostat had the highest HDAC10 affinity in the panel of drugs ($pK_d^{app\ HDAC10}$ = 7.8 vs. $pK_d^{app\ HDAC1}$ = 6.1) in sharp contrast to the original report (pK_i^{HDAC10} = 7.6 vs. pK_i^{HDAC1} = 8.2)[37].

Our assay also questions purported HDAC6 selective molecules such as Tubacin, Nexturastat A, Tubastatin A (see above), and others as appropriate chemical probes (Fig. 2d). For instance, Nexturastat A showed no substantial differences in affinity between HDAC6 and HDAC10 ($pK_d^{app\ HDAC6}$ = 6.4 vs. $pK_d^{app\ HDAC10}$ = 6.0), contrasting reported values (pEC_{50}^{HDAC6} = 8.3 vs. pEC_{50}^{HDAC10} = 5.1)[38], but in line with recently reported nano-BRET data[36]. Furthermore, Nexturastat A also potently engages MBLAC2 (pK_d^{app} = 7.6), a novel finding that reduces the drugs' apparent selectivity. Even more intriguingly, the two clinical designated HDAC6 inhibitors Ricolinostat and Citarinostat showed only 7-25-fold preferred binding for HDAC6 over class I HDACs, resulting in poor selectivity scores (Fig. 2d). Among all HDAC6-binding molecules, ACY-738 was the only compound with a perfect CATDS score of 1 (Fig. 2d). The selectivity of its close analogue ACY-775 was much lower (CATDS = 0.52) owing to the nearly equipotent binding of MBLAC2. Considering this exquisite selectivity and its submicromolar affinity, ACY-738 currently appears to be the chemical probe of choice for HDAC6.

HDACi target engagement depends on the composition of HDAC complexes. HDACs exert their functions as part of protein complexes and when tight complexes are formed, endogenously interacting proteins are captured by the affinity matrix. This allowed to interrogate the binding of HDACis to the five major known HDAC complexes systematically. The CoREST, NuRD, Sin3 and MiDAC complex are formed around a core of 1-2 isoforms of HDAC1 or HDAC2, while the NCoR complex is formed around HDAC3[39]. In accordance to published results[17, 18], we found the association of HDAC3 with NCoR complex partners to not generally affect K_d^{app} values for any of the inhibitor chemotypes (Fig. S9). Regarding HDAC1 and HDAC2-based complexes, however, we observed impact of the HDAC interactome on the drug affinity. For instance, Trichostatin A showed a 14-fold EC_{50} difference (ΔpEC_{50}) between HDAC1 and the MiDAC

component DNTTIP1, indicating that Trichostatin A preferentially binds to HDAC1 when part of the MiDAC complex (Fig. 3a). Even more strikingly, RCOR3 repeatedly showed an >10-fold lower EC_{50} value compared to RCOR1 and other CoREST members, which was observed most prominently for Panobinostat, Romidepsin, Dacinostat and M344 (Fig. 3b). These measurements support the existence of drug selectivity between variants of the same complex depending on its (mutually exclusive) subunits. To generalize the above, we calculated ΔpEC_{50} for HDAC1 and each complex protein (Fig. 3c). This led to the clear distinction between aminoanilides and the other drugs: aminoanilides showed decreased potency (ΔpEC_{50} coloured in red) while other drugs showed increased potency (ΔpEC_{50} coloured in blue) for HDACs when part of complexes. Enhanced affinity to RCOR3-interacting HDACs was observed for the majority of hydroxamic acid inhibitors. In contrast, aminoanilides appeared to interact only weakly with HDAC1/2 when involved in a complex, as deduced from the negative ΔpEC_{50}. These data confirm and extend previous observations that HDACi target engagement depends on the composition of HDAC complexes and thus provides prospects for the development of further HDAC complex-specific drugs.

The acyl-CoA hydrolase MBLAC2 is a common and potent off-target of HDACis. The perhaps most unexpected result of this study was the observation of MBLAC2 as an off-target of 24 hydroxamate molecules (Fig. 2). Amongst those are approved drugs such as Panobinostat (pK_d^{app} = 5.9) and frequently used tool compounds such as Nexturastat A (pK_d^{app}= 7.6) (Fig. 4a). To ascertain that inhibition of binding equals inhibition of enzymatic activity, we deployed a recombinant enzyme activity assay based on the MBLAC2-catalyzed hydrolysis of ^{3}H-labeled palmitoyl-CoA (Fig. 4b)[23]. MBLAC2 activity was affected by nearly all binders at 300 nM drug concentration and reduced to background for 18 HDACis (Fig. 4c). HDAC drugs (e.g. Tucidinostat, PCI-34051) that showed no or very weak MBLAC2 binding in the chemoproteomic assay, at most, only slightly reduced enzyme activity of MBLAC2. Full dose-response assays for 11 compounds determined that most hit the experimental EC_{50} limit of 5-10 nM (i.e. pEC_{50} of ca. 8.0-8.3), which corresponds to 50% of the applied enzyme concentration. Notably, these potent inhibitors included the approved drug Panobinostat (pEC_{50} > 8.0) and the orphan drug Pracinostat (pEC_{50} > 8.2) (Fig. 4d, S10). In contrast, the approved aminoanilide Tucidinostat did not affect MBLAC2 activity even at a 1000-fold higher concentration. Also in concordance with the competition binding data, ACY-775 (pK_d^{app} = 6.1, pEC_{50} = 8.2) is a very potent MBLAC2 inhibitor, while the chemically closely related compound ACY-738 (pK_d^{app} < 4.5, pEC_{50} = 6.3) is >75-fold less potent (Fig. 4e).

MBLAC2 inhibition induces accumulation of extracellular vesicles. MBLAC2 is a poorly characterized protein. Yet, it has been shown to interact with the palmitoyltransferase ZDHHC20[23], a regulator of endocytosis-mediated EGFR internalization[40], as well as other proteins (BioPlex)[41-43] whose GO term enrichment hints at roles in endo- or exocytosis (Table S3). Concurring GO annotations were also found when analysing the localisation and roles of MBLAC2-coregulated proteins (proteomeHD)[44] (Table S3). In addition, HDAC6 inhibitor Tubacin has been shown to produce a strong vesicle phenotype that cannot be attributed to HDAC6 inhibition[45]. Since we identified Tubacin to inhibit MBLAC2 (Fig. 2a, 4c), we speculated that the vesicle phenotype may be related to MBLAC2 activity. Knocking down (KD) >85%

of the protein in HEK293 cells using siRNA did not have a substantial effect on the expression of 7112 monitored proteins including those known to be associated with MBLAC2 and vesicle biology (Fig. S11a,b, Table S4). However, the knockdown indeed induced accumulation of extracellular vesicles in the cell culture supernatants (Fig. 5a). The accumulation was even more pronounced upon pharmacological inhibition of MBLAC2 with ACY775 (Fig. 5b, a dual MBLAC2 and HDAC6 inhibitor), compared to treatment with its close analogue ACY738 (an HDAC6 but not an MBLAC2 inhibitor at the used concentration, Fig. 1). Together, these data show for the first time, that MBLAC2 activity regulates extracellular vesicle levels, either as a negative regulator of vesicle formation or as a positive regulator of vesicle uptake.

Considering the involvement of lipids and particularly ceramides in vesicle budding[46], we wondered whether MBLAC2 hydrolase functionality (see Fig. 4b) would have an observable effect on lipids. We therefore performed an untargeted mass spectrometry-based lipidomics experiment following MBLAC2 knock-down. We observed changes in the levels of several lipids: notably hexosylceramides were significantly downregulated but sphingomyelins were generally upregulated (Fig. 5c, S11c, Table S5). While we could not demonstrate ceramidase activity of MBLAC2 when using a fluorescently labelled C12-ceramide model substrate (Fig. S11d-g), the observed changes in lipid composition may still be the direct or indirect result of inhibiting one or several MBLAC2 activities.

Discussion

The current study makes several noteworthy contributions to the field of chemical biology. The profiling data for the 53 drugs targeting HDACs and metallohydrolases is a rich resource for chemical biologists and medicinal chemists that we make available here and in ProteomicsDB for further interrogation by the scientific community. The study not only substantially extends the available chemoproteomic data beyond the 16 HDACis previously analysed in a conceptually similar way[17], it also compares favourably to the hitherto largest studies using other profiling technologies [34, 35]. This extensive scope enabled analyses not possible in small data sets and revealed a number of surprises.

First, the novel mixed affinity matrix goes beyond the state of the art[17, 20, 26, 47-49] as it enriches 9 out of the 11 human zinc-dependent HDACs including class IIa HDACs. This improvement mostly stems from the development of iC, which exploits the published diarylcyclopropane-hydroxamic acid chemotype developed for HDAC5 inhibition[50, 51]. In this series of inhibitors, enantiomerically pure CHDI00465983 is class IIa selective (Fig. 2), while iC advantageously exhibits pan-HDAC binding character (Fig. S1). This large target space may be explained by the isomeric composition of the triazole affinity matrix, which comprises 3 enantiomer pairs (Fig. S1 and methods). Immobilised Quisinostat, iQ, enriches HDAC8 better than immobilized Vorinostat (6) or any other affinity matrix tested. A posteriori, it is noticeable that iC and iA were required for the robust enrichment of the off-targets MBLAC2 and GATD3A, ALDH2, ISOC1, and ISOC2 respectively. The design of iA, a simple alkyl chain terminated by an hydroxamate, has considerable future potential for profiling metalloproteins. We hypothesise that the sterically permissive alkyl chain, also found in all HDACis constituting group B (Fig. 2a, S6), can position the metal-binding

group in the active sites of many metalloproteins supporting their enrichment. Despite these improvements, HDAC9 and HDAC11 currently remain out of reach. iC is likely a HDAC9 binder owing to the structural similarities of HDAC9 and HDAC5. However, interrogating hundreds of cell line proteomes[27-29] did not identify a cell line rich enough in HDAC9 or otherwise practical for inclusion in our assay. HDAC11 is also very scarce and the structure of its active pocket, adapted to its preference for long acyl chains, limits the cross-reactivity of this sole member of class IV HDACs[52-54]. Inclusion of this enzyme in our assay will therefore require both an adapted cell line and dedicated probe. As it stands, owing to its broad metalloprotein coverage, our mixed matrix will not only serve the profiling of human HDAC drugs, but shall also be used to interrogate e.g. parasitic metalloproteins. HDACs are indeed particularly well preserved across the species phylogeny, which supports the concept of repurposing human drugs against parasites such as *Schistosoma Mansoni* or *Plasmodium Falciparum*[55].

Second, it is obviously important to know which proteins are engaged by a given drug, how potent it is for that target and what its selectivity over other targets is to be able to attribute an observed biological effect to the target(s) of the compound. For example, for the designated HDAC6 inhibitors Ricolinostat ($pK_d^{app\ HDAC6}$ = 7.1) and Citarinostat ($pK_d^{app\ HDAC6}$ = 6.7), our data indicate a narrow selectivity window consistent with an earlier study suggesting that their anti-cancer effects mainly stem from the inhibition of HDACs 1-3 (pK_d^{app} range of 4.9-6.0, Fig. 1) rather than HDAC6[56]. More surprisingly, Tubastatin A has been used in >100 publications to probe HDAC6 biology under the assumption that it is a selective HDAC6 inhibitor[34]. According to our results however, Tubastatin A has a higher potency for HDAC10 than HDAC6 ($pK_d^{app\ HDAC10}$ = 7.5 vs. $pK_d^{app\ HDAC6}$ = 5.0). We hypothesize that the discrepancy between the published HDAC activity inhibition data and our chemoproteomic binding data as well as in-cell target engagement data using nanoBRET[36], originate from the inadequacy of the peptidic substrate used in early studies: HDAC10 was only recently annotated as a polyamine rather than protein deacylase[57]. In this regard, it is noteworthy that the most potent HDAC10 binders in our assay (Tubastatin A, Abexinostat, Pracinostat, Quisinostat, Panobinostat, Dacinostat, see Fig. S6) feature a positively charged aminogroup which may mimic an interaction between a polyamine and the gatekeeper glutamate (Glu^{272} or potentially Glu^{22}) of HDAC10[36]. The chemoproteomic data also demonstrate that it is possible to achieve high selectivity and three of the profiled drugs even fulfil prime criteria for a chemical probe (sub-micromolar potency, 30-fold window over other targets)[58]. More specifically, these are ACY-738 for HDAC6, PCI-34051 for HDAC8 and TH65 for HDAC10 (see Table S1).

Third, it is evident from the target landscape, that the design of inhibitors that discriminate between the very similar active sites of HDAC1,2 and HDAC3 is challenging. It has, however, been shown that selectivity may come from designing drugs that target particular HDAC complexes[39], with a particular interest for CoREST-selective HDACi to treat synaptopathies[59]. Chemoproteomic profiling preserves HDAC complexes which led to the observation that hydroxamic acid drugs tend to prefer binding to CoREST, Sin3 and MiDAC complexes (Fig. 3c). Surprisingly, some of those drugs bind with >10-fold higher affinity to HDAC1 or HDAC2 when interacting with RCOR3 instead of the alternative CoREST

subunit RCOR1. In contrast to hydroxamates, aminoanilide drugs appear to bind better to HDACs that are not part of a complex. One may speculate that HDACs in complexes may adopt a conformation unable to accommodate the bulky aminoanilide zinc binding group. The binding of aminoanilides to free HDACs would then hinder complex formation by locking the HDAC in a conformation unfavourable of interaction partner binding. Due to their slow k_{off} rate[18, 24], aminoanilides might therefore sequester HDACs particularly from temporary formed complexes such as the MiDAC complex. As a result, different classes of HDAC drugs might modulate the acetylation status of HDAC substrate proteins differentially, depending on whether they preferentially engage one of the complexes or the HDACs in isolation.

Fourth, one of the most exciting outcomes of chemoproteomic profiling experiments is the identification of unexpected targets for otherwise well characterized drugs. For instance, we and others have identified novel targets of kinase inhibitors within (e.g. activin receptor ALK2 for the ATM inhibitor CP466722)[60] or outside the target class (e. g. ferrochelatase for the BRAF inhibitor Vemurafenib and others)[61]. The current study, uncovered five such cases for HDAC inhibitors, notably ALDH2 (n=9 drugs, most potent pK_d^{app} = 6.5), GATD3A (n=7 drugs, most potent pK_d^{app} = 5.8), ISOC1 (n=7 drugs, most potent pK_d^{app} = 6.8), ISOC2 (n=8 drugs, most potent pK_d^{app} = 8.2) and MBLAC2 (n=24 drugs, most potent pK_d^{app} = 7.6). Interestingly, MBLAC2 was bound by several HDACi classes. The other off-targets seem to be preferentially bound by HDACis whose hydroxamic acid is presented via an alkyl chain. Hence, the alkyl may favour off-target binding while HDACis with conjugated or aromatic linkers will be more selective for HDACs (group C, Fig. 2a). All off-targets but ALDH2 are poorly characterized proteins and it remains to be investigated whether HDACi binding affects their biological function and thus impacts drug efficacy. Intriguingly, ISOC1 knockdown has been reported to inhibit cancer cell proliferation and metastasis[62, 63], which may be a desirable off-target effect of e. g. Vorinostat. Droxinostat and Bufexamac did not bind HDACs in our assay but some of the off-targets, which may allow to repurpose these molecules to probe the function of these proteins.

Fifth, among the non-HDAC off-targets, MBLAC2 stands out for its potent and frequent binding to hydroxamic acid HDAC inhibitors. This protein has recently been shown to hydrolyse acyl-CoA and just like HDACs utilizes Zn^{2+} for catalysis[23]. Our data shows for the first time that HDACis can inhibit the palmitoyl-CoA hydrolase function of the enzyme in vitro and several do so with single digit nano-molar EC_{50}s (pEC_{50} > 8.0). Interestingly, a study describing an HDAC6-independent Tubacin stimulatory effect on exosome biogenesis[45] led us to hypothesise that this phenotype may stem from the inhibition of MBLAC2, the only off-target of Tubacin in our chemoproteomic assay. Similarly, an unexplained phenotype was reported for AR42[64], which we identified as a potent MBLAC2 inhibitor: AR42 leads to upregulation of ceramide levels[64], a known trigger of exosome biogenesis[46]. Given that MBLAC2 can hydrolyze palmitoyl-CoA, the initial building block of ceramides, we speculated that MBLAC2 might be involved in regulating ceramide levels and exosome release. In line with such a putative role, the BioPlex database[41-43] reports MBLAC2 as an interactor of proteins involved in vesicle formation and trafficking and prior bioinformatic analysis has suggested MBLAC2 expression to be co-regulated with

proteins involved in exosome biogenesis (e.g. TSG101, VPS28, ANXA7)[44]. Proteome profiling of HEK293 cells in response to MBLAC2 knock-down did not confirm latter coregulation and we could also not obtain direct evidence for ceramidase activity using a C12-ceramide substrate in vitro. This does not rule out the possibility that MBLAC2 hydrolyzes certain ceramides or other lipids in cells. Such a lipidase functionality has indeed been elucidated for at least one of the 18 human metallo-beta-lactamase domain containing proteins[65], i.e. N-acyl-phosphatidylethanolamine-hydrolyzing phospholipase D (NAPEPLD)[66-68]. In fact, MBLAC2 knockdown had an effect on intracellular concentrations of some lipid families, including a general decrease of hexosylceramide and concomitant increase of sphingomyeline levels. Phenotypically, we could demonstrate a strong accumulation of extracellular vesicles when MBLAC2 was knocked down or pharmacologically inhibited in HEK293 cells. Together, these results substantiate a role of MBLAC2 in extracellular vesicles biology and prove that the protein can be addressed by small molecule drugs. Further work is required to delineate whether MBLAC2 inhibition causes biologically or therapeutically important systemic or local effects. For instance, a large body of literature portraits a plethora of ways in which cancer cells make use of exosomes to establish metastatic niches or fight the immune system[69-75]. On the other hand, the immune system
relies on exosomes and cancer exosome release might stimulate immune responses[76-79]. To understand such potential effects of MBLAC2 inhibition on clinical outcome and human physiology, one can also envisage isolating vesicles from e.g. human plasma collected in HDACi clinical trials (e. g. MBLAC2/HDAC inhibitor Pracinostat vs. placebo) to investigate a systemic effect of MBLAC2 inhibition. Because the inhibitors we found to be dual HDAC6/MBLAC2 inhibitors are investigated in neurological diseases, for instance to improve axonal transport of brain-derived neurotrophic factor (BDNF) vesicles and BDNF release[80, 81], it is tempting to hypothesise about a synergy between MBLAC2 vesicle regulations (increased release) and HDAC6-linked effects on microtubular vesicle transport and fusion (improved transport to release location)[5, 82, 83]. Should MBLAC2 emerge as a bona fide drug target, several HDACis presented here could be repurposed to stimulate targeted exosome release.

To conclude, this study has shown how the design and synthesis of promiscuous affinity probes enabled the delineation of the target landscape of HDACis. The drug profiles, assembled in the freely accessible online database ProteomicsDB, inform medicinal chemistry and highlight chemical probes to study biology. The surprising identification of MBLAC2 as an HDACi target helped placing this poorly characterized protein into a functional context and may provide the basis for future drug discovery programs focussed on vesicle pathobiology.

Declarations

Acknowledgements

We want to thank Wendy Greentree (Cornell) for technical support and Laura Wanat (TUM). We gratefully acknowledge funding by the Deutsche Forschungsgemeinschaft (DFG) for S.L. (SFB 1309, project 401883058) and P.P. (project 407391208). M.I.P.M. and M.E.L. acknowledge support from the National

Institutes of Health (grant GM121540). Contributions by V.W. and J.K.P. are funded by the Bavarian State Ministry of Science and the Arts within the framework of the Bavarian Research Institute for Digital Transformation (bidt).

References

1. Bettica, P. *et al.* Histological effects of givinostat in boys with Duchenne muscular dystrophy. *Neuromuscul Disord* **26**, 643-649 (2016).

2. Marks, P.A. & Breslow, R. Dimethyl sulfoxide to vorinostat: development of this histone deacetylase inhibitor as an anticancer drug. *Nat Biotechnol* **25**, 84-90 (2007).

3. Li, Y. & Seto, E. HDACs and HDAC Inhibitors in Cancer Development and Therapy. *Cold Spring Harb Perspect Med* **6** (2016).

4. Hayashi, A. *et al.* Type-specific roles of histone deacetylase (HDAC) overexpression in ovarian carcinoma: HDAC1 enhances cell proliferation and HDAC3 stimulates cell migration with downregulation of E-cadherin. *Int J Cancer* **127**, 1332-1346 (2010).

5. Guo, W. *et al.* HDAC6 inhibition reverses axonal transport defects in motor neurons derived from FUS-ALS patients. *Nat Commun* **8**, 861 (2017).

6. Saito, M. *et al.* Acetylation of intrinsically disordered regions regulates phase separation. *Nat Chem Biol* **15**, 51-61 (2019).

7. Federspiel, J.D., Greco, T.M., Lum, K.K. & Cristea, I.M. Hdac4 Interactions in Huntington's Disease Viewed Through the Prism of Multiomics. *Mol Cell Proteomics* **18**, S92-S113 (2019).

8. Mielcarek, M. *et al.* HDAC4 reduction: a novel therapeutic strategy to target cytoplasmic huntingtin and ameliorate neurodegeneration. *PLoS Biol* **11**, e1001717 (2013).

9. Chang, L., Ruiz, P., Ito, T. & Sellers, W.R. Targeting pan-essential genes in cancer: Challenges and opportunities. *Cancer Cell* **39**, 466-479 (2021).

10. Subramanian, S., Bates, S.E., Wright, J.J., Espinoza-Delgado, I. & Piekarz, R.L. Clinical Toxicities of Histone Deacetylase Inhibitors. *Pharmaceuticals (Basel)* **3**, 2751-2767 (2010).

11. Balasubramanian, S., Verner, E. & Buggy, J.J. Isoform-specific histone deacetylase inhibitors: the next step? *Cancer Lett* **280**, 211-221 (2009).

12. Bardai, F.H. & D'Mello, S.R. Selective toxicity by HDAC3 in neurons: regulation by Akt and GSK3beta. *J Neurosci* **31**, 1746-1751 (2011).

13. Zhang, X. *et al.* Histone deacetylase 3 (HDAC3) activity is regulated by interaction with protein serine/threonine phosphatase 4. *Genes Dev* **19**, 827-839 (2005).

14. Millard, C.J. *et al.* Class I HDACs share a common mechanism of regulation by inositol phosphates. *Mol Cell* **51**, 57-67 (2013).

15. Watson, P.J. *et al.* Insights into the activation mechanism of class I HDAC complexes by inositol phosphates. *Nat Commun* **7**, 11262 (2016).

16. Guenther, M.G., Barak, O. & Lazar, M.A. The SMRT and N-CoR corepressors are activating cofactors for histone deacetylase 3. *Mol Cell Biol* **21**, 6091-6101 (2001).

17. Bantscheff, M. *et al.* Chemoproteomics profiling of HDAC inhibitors reveals selective targeting of HDAC complexes. *Nat Biotechnol* **29**, 255-265 (2011).

18. Becher, I. *et al.* Chemoproteomics reveals time-dependent binding of histone deacetylase inhibitors to endogenous repressor complexes. *ACS Chem Biol* **9**, 1736-1746 (2014).

19. Turnbull, R.E. *et al.* The MiDAC histone deacetylase complex is essential for embryonic development and has a unique multivalent structure. *Nat Commun* **11**, 3252 (2020).

20. Weigt, D., Hopf, C. & Medard, G. Studying epigenetic complexes and their inhibitors with the proteomics toolbox. *Clin Epigenetics* **8**, 76 (2016).

21. Hu, T. *et al.* HDAC5 catalytic activity suppresses cardiomyocyte oxidative stress and NRF2 target gene expression. *J Biol Chem* **294**, 8640-8652 (2019).

22. Kikuchi, S. *et al.* Class IIa HDAC inhibition enhances ER stress-mediated cell death in multiple myeloma. *Leukemia* **29**, 1918-1927 (2015).

23. Malgapo, M.I.P., Safadi, J.M. & Linder, M.E. Metallo-beta-lactamase domain-containing protein 2 is S-palmitoylated and exhibits acyl-CoA hydrolase activity. *J Biol Chem* **296**, 100106 (2020).

24. Robers, M.B. *et al.* Target engagement and drug residence time can be observed in living cells with BRET. *Nat Commun* **6**, 10091 (2015).

25. Bradner, J.E. *et al.* Chemical phylogenetics of histone deacetylases. *Nat Chem Biol* **6**, 238-243 (2010).

26. Becher, I. *et al.* Thermal profiling reveals phenylalanine hydroxylase as an off-target of panobinostat. *Nat Chem Biol* **12**, 908-910 (2016).

27. Samaras, P. *et al.* ProteomicsDB: a multi-omics and multi-organism resource for life science research. *Nucleic Acids Res* **48**, D1153-D1163 (2020).

28. Schmidt, T. *et al.* ProteomicsDB. *Nucleic Acids Res* **46**, D1271-D1281 (2018).

29. Wilhelm, M. *et al.* Mass-spectrometry-based draft of the human proteome. *Nature* **509**, 582-587 (2014).

30. Heinzlmeir, S. *et al.* Chemoproteomics-Aided Medicinal Chemistry for the Discovery of EPHA2 Inhibitors. *ChemMedChem* **12**, 999-1011 (2017).

31. Balasubramanian, S. *et al.* A novel histone deacetylase 8 (HDAC8)-specific inhibitor PCI-34051 induces apoptosis in T-cell lymphomas. *Leukemia* **22**, 1026-1034 (2008).

32. Heimburg, T. *et al.* Structure-Based Design and Synthesis of Novel Inhibitors Targeting HDAC8 from Schistosoma mansoni for the Treatment of Schistosomiasis. *J Med Chem* **59**, 2423-2435 (2016).

33. Heimburg, T. *et al.* Structure-Based Design and Biological Characterization of Selective Histone Deacetylase 8 (HDAC8) Inhibitors with Anti-Neuroblastoma Activity. *J Med Chem* **60**, 10188-10204 (2017).

34. Butler, K.V. *et al.* Rational design and simple chemistry yield a superior, neuroprotective HDAC6 inhibitor, tubastatin A. *J Am Chem Soc* **132**, 10842-10846 (2010).

35. Shen, S. *et al.* Structural and in Vivo Characterization of Tubastatin A, a Widely Used Histone Deacetylase 6 Inhibitor. *ACS Med Chem Lett* **11**, 706-712 (2020).

36. Geraldy, M. *et al.* Selective Inhibition of Histone Deacetylase 10: Hydrogen Bonding to the Gatekeeper Residue is Implicated. *J Med Chem* **62**, 4426-4443 (2019).

37. Buggy, J.J. *et al.* CRA-024781: a novel synthetic inhibitor of histone deacetylase enzymes with antitumor activity in vitro and in vivo. *Mol Cancer Ther* **5**, 1309-1317 (2006).

38. Bergman, J.A. *et al.* Selective histone deacetylase 6 inhibitors bearing substituted urea linkers inhibit melanoma cell growth. *J Med Chem* **55**, 9891-9899 (2012).

39. Millard, C.J., Watson, P.J., Fairall, L. & Schwabe, J.W.R. Targeting Class I Histone Deacetylases in a "Complex" Environment. *Trends Pharmacol Sci* **38**, 363-377 (2017).

40. Runkle, K.B. *et al.* Inhibition of DHHC20-Mediated EGFR Palmitoylation Creates a Dependence on EGFR Signaling. *Mol Cell* **62**, 385-396 (2016).

41. Huttlin, E.L. *et al.* Dual proteome-scale networks reveal cell-specific remodeling of the human interactome. *Cell* **184**, 3022-3040 e3028 (2021).

42. Huttlin, E.L. *et al.* Architecture of the human interactome defines protein communities and disease networks. *Nature* **545**, 505-509 (2017).

43. Huttlin, E.L. *et al.* The BioPlex Network: A Systematic Exploration of the Human Interactome. *Cell* **162**, 425-440 (2015).

44. Kustatscher, G. *et al.* Co-regulation map of the human proteome enables identification of protein functions. *Nat Biotechnol* **37**, 1361-1371 (2019).

45. Chao, O.S. *et al.* The HDAC6 Inhibitor Tubacin Induces Release of CD133(+) Extracellular Vesicles From Cancer Cells. *J Cell Biochem* **118**, 4414-4424 (2017).

46. Trajkovic, K. *et al.* Ceramide triggers budding of exosome vesicles into multivesicular endosomes. *Science* **319**, 1244-1247 (2008).

47. Lobera, M. *et al.* Selective class IIa histone deacetylase inhibition via a nonchelating zinc-binding group. *Nat Chem Biol* **9**, 319-325 (2013).

48. Albrow, V.E. *et al.* Design and development of histone deacetylase (HDAC) chemical probes for cell-based profiling. *Mol Biosyst* **12**, 1781-1789 (2016).

49. Fischer, J.J. *et al.* SAHA Capture Compound--a novel tool for the profiling of histone deacetylases and the identification of additional vorinostat binders. *Proteomics* **11**, 4096-4104 (2011).

50. Burli, R.W. *et al.* Design, synthesis, and biological evaluation of potent and selective class IIa histone deacetylase (HDAC) inhibitors as a potential therapy for Huntington's disease. *J Med Chem* **56**, 9934-9954 (2013).

51. Luckhurst, C.A. *et al.* Potent, Selective, and CNS-Penetrant Tetrasubstituted Cyclopropane Class IIa Histone Deacetylase (HDAC) Inhibitors. *ACS Med Chem Lett* **7**, 34-39 (2016).

52. Kutil, Z. *et al.* Continuous Activity Assay for HDAC11 Enabling Reevaluation of HDAC Inhibitors. *ACS Omega* **4**, 19895-19904 (2019).

53. Moreno-Yruela, C., Galleano, I., Madsen, A.S. & Olsen, C.A. Histone Deacetylase 11 Is an epsilon-N-Myristoyllysine Hydrolase. *Cell Chem Biol* **25**, 849-856 e848 (2018).

54. Liu, S.S., Wu, F., Jin, Y.M., Chang, W.Q. & Xu, T.M. HDAC11: a rising star in epigenetics. *Biomed Pharmacother* **131**, 110607 (2020).

55. Hailu, G.S. *et al.* Lysine Deacetylase Inhibitors in Parasites: Past, Present, and Future Perspectives. *J Med Chem* **60**, 4780-4804 (2017).

56. Lin, A. *et al.* Off-target toxicity is a common mechanism of action of cancer drugs undergoing clinical trials. *Sci Transl Med* **11** (2019).

57. Hai, Y., Shinsky, S.A., Porter, N.J. & Christianson, D.W. Histone deacetylase 10 structure and molecular function as a polyamine deacetylase. *Nat Commun* **8**, 15368 (2017).

58. Arrowsmith, C.H. *et al.* The promise and peril of chemical probes. *Nat Chem Biol* **11**, 536-541 (2015).

59. Fuller, N.O. *et al.* CoREST Complex-Selective Histone Deacetylase Inhibitors Show Prosynaptic Effects and an Improved Safety Profile To Enable Treatment of Synaptopathies. *ACS Chem Neurosci* **10**, 1729-1743 (2019).

60. Reinecke, M. *et al.* Chemoproteomic Selectivity Profiling of PIKK and PI3K Kinase Inhibitors. *ACS Chem Biol* **14**, 655-664 (2019).

61. Klaeger, S. *et al.* Chemical Proteomics Reveals Ferrochelatase as a Common Off-target of Kinase Inhibitors. *ACS Chem Biol* **11**, 1245-1254 (2016).

62. Cheng, L., Zhao, Y., Tang, M., Luo, Z. & Wang, X. Knockdown of ISOC1 suppresses cell proliferation in pancreatic cancer in vitro. *Oncol Lett* **17**, 4263-4270 (2019).

63. Gao, B. *et al.* Knockdown of ISOC1 inhibits the proliferation and migration and induces the apoptosis of colon cancer cells through the AKT/GSK-3beta pathway. *Carcinogenesis* **41**, 1123-1133 (2020).

64. Xu, W., Xu, B., Yao, Y., Yu, X. & Shen, J. The novel HDAC inhibitor AR-42-induced anti-colon cancer cell activity is associated with ceramide production. *Biochem Biophys Res Commun* **463**, 545-550 (2015).

65. Pettinati, I., Brem, J., Lee, S.Y., McHugh, P.J. & Schofield, C.J. The Chemical Biology of Human Metallo-beta-Lactamase Fold Proteins. *Trends Biochem Sci* **41**, 338-355 (2016).

66. Okamoto, Y., Morishita, J., Tsuboi, K., Tonai, T. & Ueda, N. Molecular characterization of a phospholipase D generating anandamide and its congeners. *J Biol Chem* **279**, 5298-5305 (2004).

67. Wang, J. *et al.* Functional analysis of the purified anandamide-generating phospholipase D as a member of the metallo-beta-lactamase family. *J Biol Chem* **281**, 12325-12335 (2006).

68. Margheritis, E. *et al.* Bile Acid Recognition by NAPE-PLD. *ACS Chem Biol* **11**, 2908-2914 (2016).

69. Costa-Silva, B. *et al.* Pancreatic cancer exosomes initiate pre-metastatic niche formation in the liver. *Nat Cell Biol* **17**, 816-826 (2015).

70. Peinado, H. *et al.* Melanoma exosomes educate bone marrow progenitor cells toward a pro-metastatic phenotype through MET. *Nat Med* **18**, 883-891 (2012).

71. Rodrigues, G. *et al.* Tumour exosomal CEMIP protein promotes cancer cell colonization in brain metastasis. *Nat Cell Biol* **21**, 1403-1412 (2019).

72. Hoshino, D. *et al.* Exosome secretion is enhanced by invadopodia and drives invasive behavior. *Cell Rep* **5**, 1159-1168 (2013).

73. Chen, G. *et al.* Exosomal PD-L1 contributes to immunosuppression and is associated with anti-PD-1 response. *Nature* **560**, 382-386 (2018).

74. Poggio, M. *et al.* Suppression of Exosomal PD-L1 Induces Systemic Anti-tumor Immunity and Memory. *Cell* **177**, 414-427 e413 (2019).

75. Capello, M. *et al.* Exosomes harbor B cell targets in pancreatic adenocarcinoma and exert decoy function against complement-mediated cytotoxicity. *Nat Commun* **10**, 254 (2019).

76. Montecalvo, A. *et al.* Exosomes as a short-range mechanism to spread alloantigen between dendritic cells during T cell allorecognition. *J Immunol* **180**, 3081-3090 (2008).

77. Andre, F. *et al.* Malignant effusions and immunogenic tumour-derived exosomes. *Lancet* **360**, 295-305 (2002).

78. Wolfers, J. *et al.* Tumor-derived exosomes are a source of shared tumor rejection antigens for CTL cross-priming. *Nat Med* **7**, 297-303 (2001).

79. Walker, J.D., Maier, C.L. & Pober, J.S. Cytomegalovirus-infected human endothelial cells can stimulate allogeneic CD4+ memory T cells by releasing antigenic exosomes. *J Immunol* **182**, 1548-1559 (2009).

80. Gold, W.A., Lacina, T.A., Cantrill, L.C. & Christodoulou, J. MeCP2 deficiency is associated with reduced levels of tubulin acetylation and can be restored using HDAC6 inhibitors. *J Mol Med (Berl)* **93**, 63-72 (2015).

81. Benoy, V. *et al.* HDAC6 is a therapeutic target in mutant GARS-induced Charcot-Marie-Tooth disease. *Brain* **141**, 673-687 (2018).

82. Brindisi, M. *et al.* Old but Gold: Tracking the New Guise of Histone Deacetylase 6 (HDAC6) Enzyme as a Biomarker and Therapeutic Target in Rare Diseases. *J Med Chem* **63**, 23-39 (2020).

83. Mo, Z. *et al.* Aberrant GlyRS-HDAC6 interaction linked to axonal transport deficits in Charcot-Marie-Tooth neuropathy. *Nat Commun* **9**, 1007 (2018).

Figures

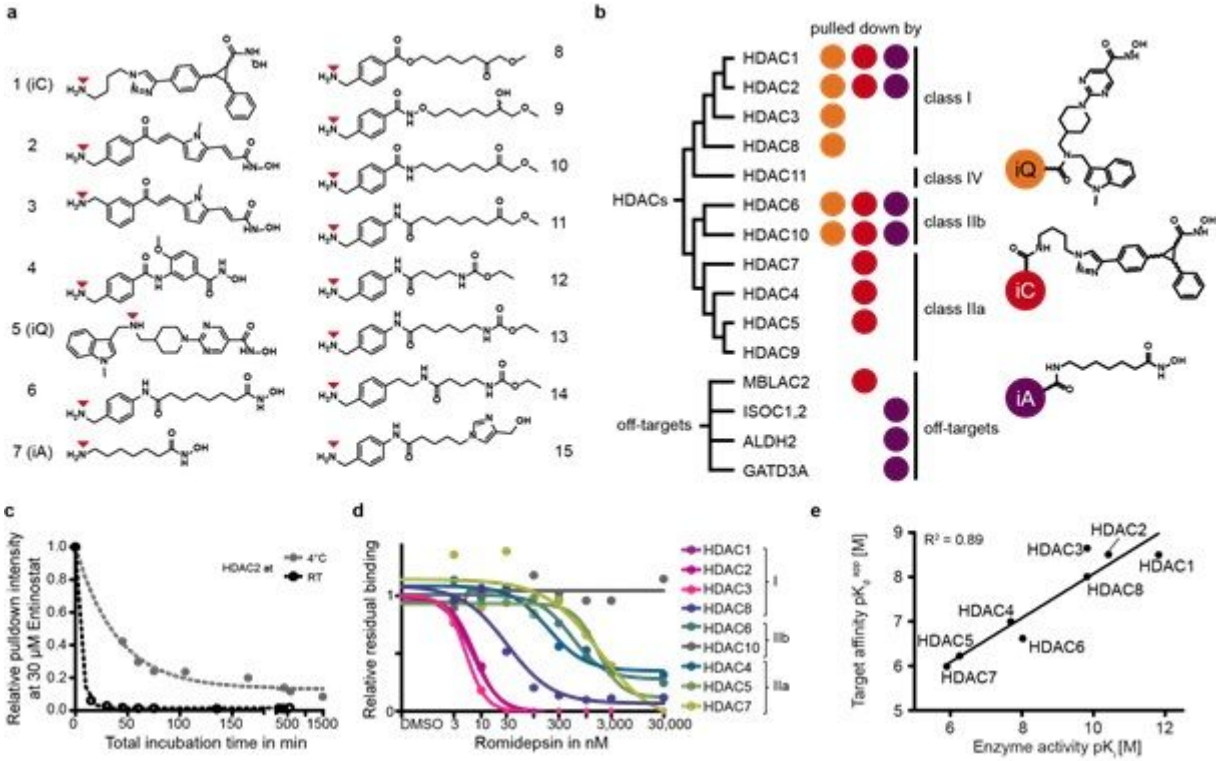

Figure 1

Chemical proteomics assay for HDAC inhibitors. a, Structures of synthesized HDAC affinity probes 1-15. Positions for on-bead immobilisation are marked with red triangles. b, Contribution of each of the three selected affinity probes to the enrichment of Zn-HDACs and off-targets. c, Time dependence of Entinostat engagement with HDAC2, using the iQ matrix at room temperature and at 4 °C. d, Exemplary dose-response curves for Romidepsin binding to HDACs using our optimized chemical proteomics assay. e, Correlation analysis between apparent dissociation constants (pKdapp, p denotes -log10) of Romidepsin: HDAC interactions determined by our chemical proteomics assay and published pKi values (-log10 of inhibitory constant) obtained by in vitro recombinant enzyme activity assays25 .

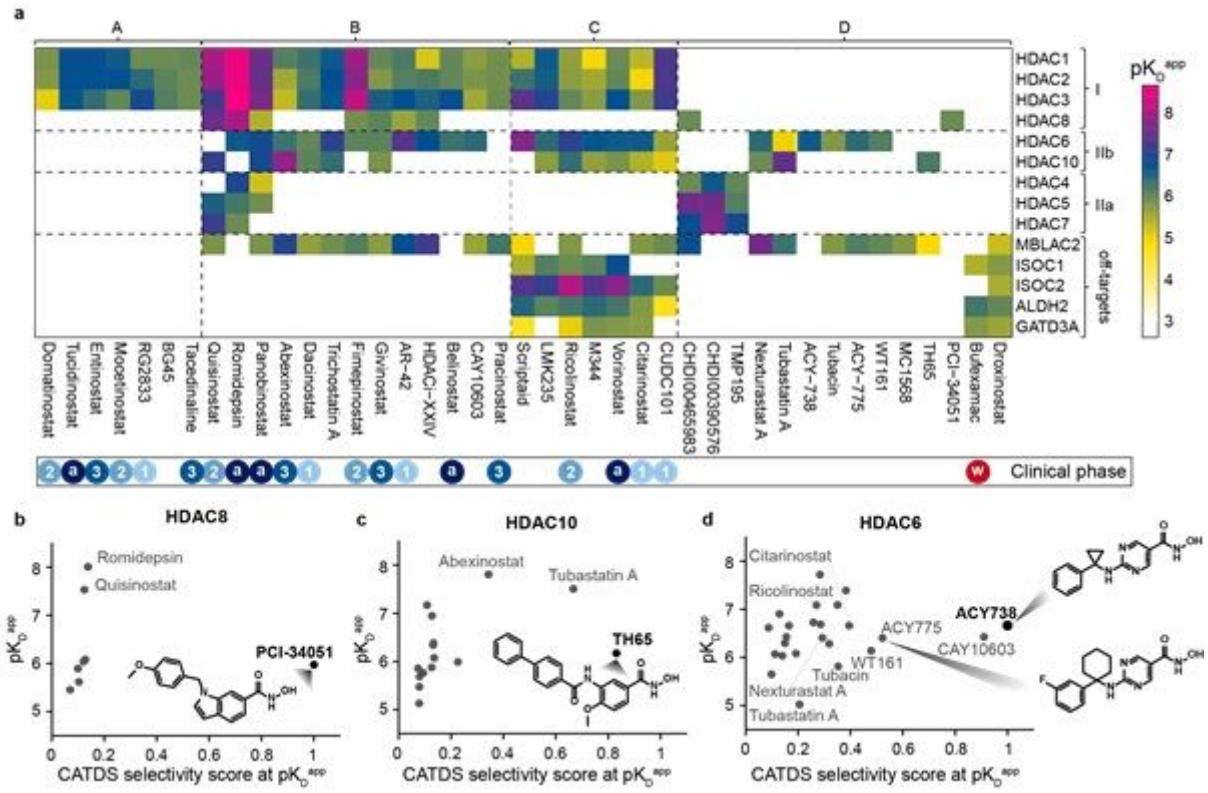

Figure 2

Target landscape of HDAC and metallohydrolase drugs. a, Heatmap of pKdapp values obtained for 41 drugs and 14 targets using chemical proteomics competition assays. A – D denotes groups of drugs that share similar target profiles. Coloured circles at the bottom of the panel indicate the status of each drug: ‘a’ is approved, ‘w’ withdrawn and ‘1-3’ phase of clinical development (1-3) (https://clue.io/repurposing-app). b-d, Scatter plots displaying the affinity of drugs binding to HDAC8, HDAC10 or HDAC6 (pKdapp) against their selectivity as measured by CATDS30 (concentration- and target-dependent selectivity; calculated for the respective target HDAC at its pKdapp, also see Fig. S8). The most selective compounds for a given target are marked by arrowheads.

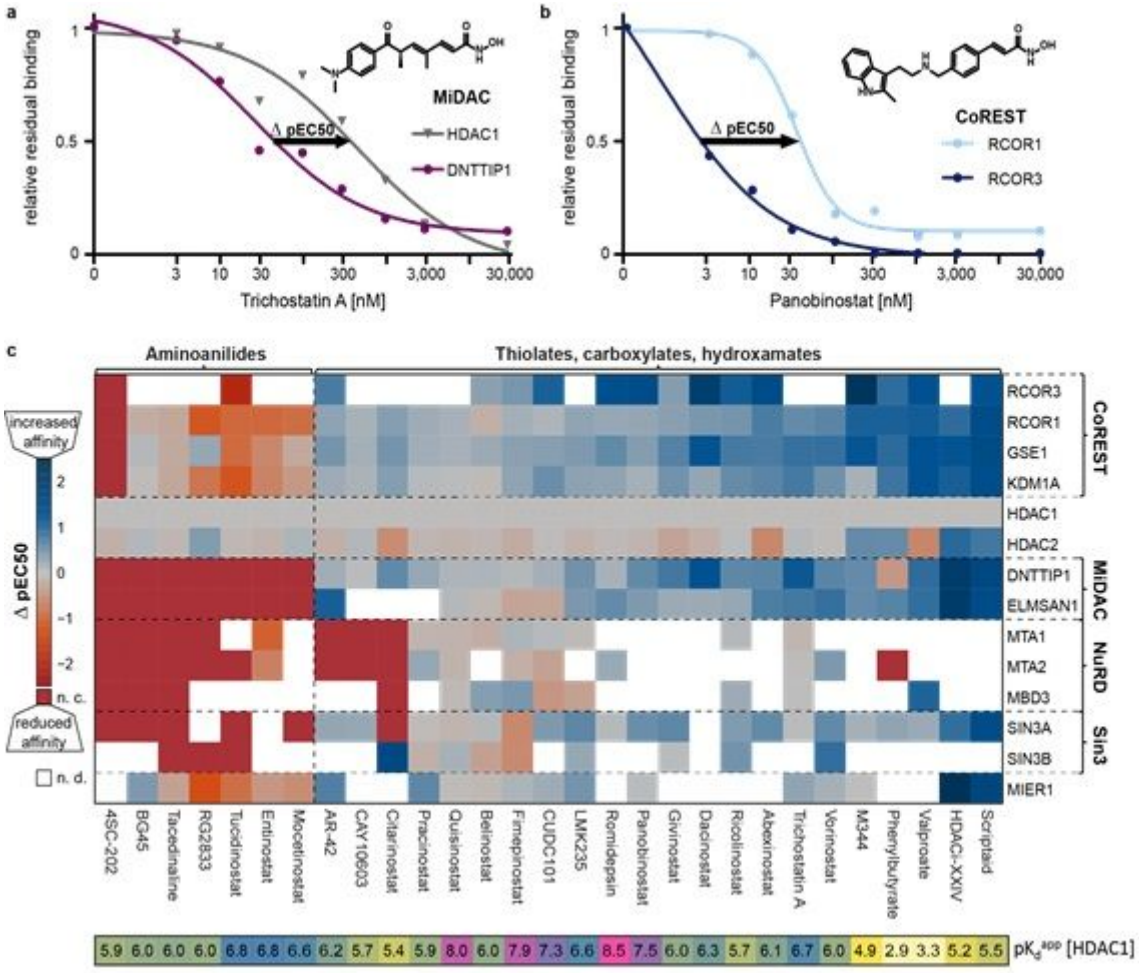

Figure 3

Complex selectivity of class I HDACis. a, Dose-response binding curves for Trichostatin A and HDAC1 and DNTTIP1 (representing the MiDAC complex). The difference between the two inflection points of dose response curves is marked by ΔpEC50 (pEC50 is -log10EC50). b, same as panel a but for Panobinostat and the CoREST subunits RCOR1 and RCOR3. c, Heatmap showing ΔpEC50 (pEC50Interactor-pEC50HDAC1) values for class I HDAC inhibitors and HDAC complex proteins. n. d. denotes that no value was determined. The bar at the bottom lists HDAC1 pKdapp values of the corresponding HDAC inhibitor.

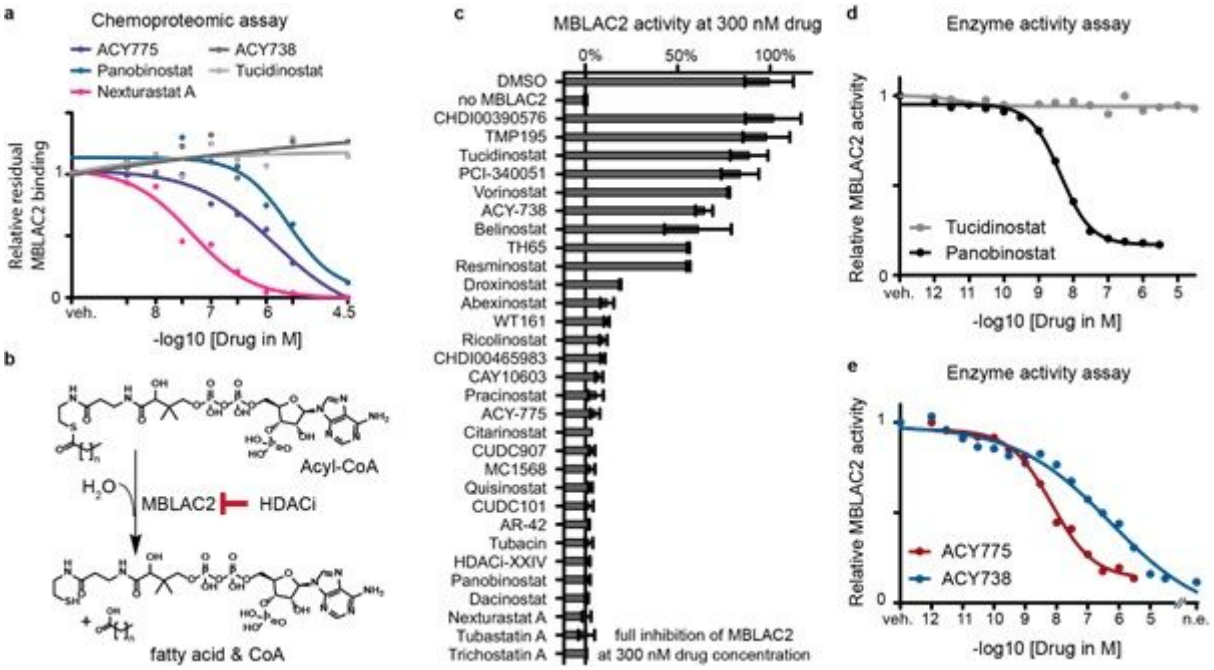

Figure 4

HDAC inhibitors abrogate MBLAC2 acyl-CoA hydrolase function at nanomolar concentrations. a, Chemoproteomic dose-response binding curve of MBLAC2 and five HDACis (veh. = vehicle control). b, Reaction schematic of MBLAC2-catalyzed hydrolysis of acyl-CoA. c, Bar plot summarizing results of a single dose MBLAC2 enzymatic inhibition screen using HDACis. Bars represent the relative rate of [3H]-palmitoyl-CoA hydrolysis in the presence of recombinant MBLAC2 (30 nM) and 24 HDACis at 300 nM drug concentration (mean of 2 measurements, whiskers of error bar denote the standard deviation). d, Dose dependent inhibition of MBLAC2 activity by approved HDACis. pEC50 denotes –log10 effective concentration). e, same as panel ‘d’ but for two structurally related compounds (n.e.= no enzyme, veh. = vehicle control).

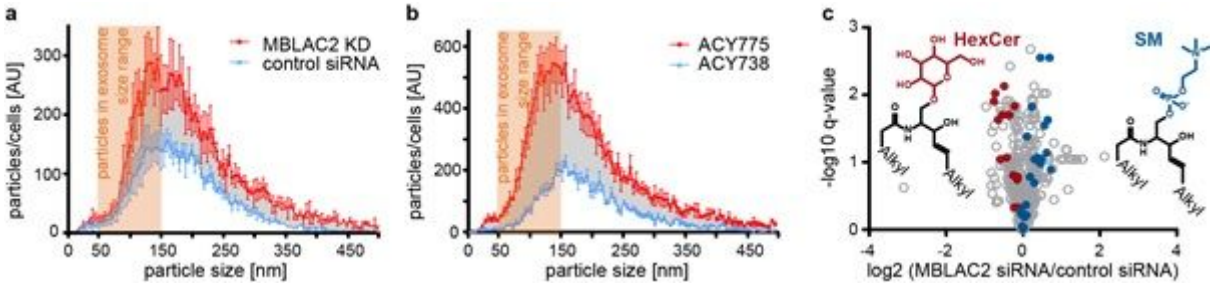

Figure 5

MBLAC2 knockdown and inhibition promote vesicle release from HEK293 cells. a, Number and size distribution of extracellular vesicles isolated from HEK293 cells treated following MBLAC2 knockdown by siRNA pools (n=3 experiments). The orange area marks the typical size range of exosomes. b, same as panel ‘a’ but for the dual HDAC6/MBLAC2 inhibitor ACY-775 (3 μM) and the selective HDAC6 inhibitor ACY-738 (3 μM). c, volcano plot summarizing the response of the lipidome of HEK293 cells in response to

MBLAC2 knockdown (n=3 experiments). Members of the hexosylceramide (HexCer) and sphingomyeline (SM) families are highlighted and their generic structures are shown.

Supplementary Files

This is a list of supplementary files associated with this preprint. Click to download.

- TableS1drugtargetlandscape.xlsx
- TableS2CATDS.xlsx
- TableS3MBLAC2GOannotations.xlsx
- TableS4proteomics.xlsx
- TableS5Lipidomics.xlsx
- SupplementaryNote.docx
- Methods.docx
- SupplementaryFigures.docx